(Received 18 February 2026, Accepted 31 March 2026, Scheduled 11 April 2026)

Design and Experimental Validation of a Wideband Patch Antenna for Ku-Band Satellite Systems Using DGS and DMS Techniques

Rajae Tribak[1,*], Hicham Setti[1], Moustapha El Bakkali[2], Aziz Dkiouak[3], and Larbi Setti[1]

[1] *RGIEAST, FPL, Abdelmalek Essaadi University, Tetouan, Morocco*
[2] *ISD Laboratory, Electronic and Smart Systems Team, Faculty of Sciences, Abdelmalek Essâadi University, Tetouan, Morocco*
[3] *STIC Laboratory, Faculty of Sciences, Chouaib Doukkali University, El Jadida, Morocco*

ABSTRACT: This research presents the design and evaluation of a high-performance Ku-band microstrip patch antenna for satellite communications. The antenna incorporates a Defected Ground Structure (DGS) and a Defected Microstrip Structure (DMS) to achieve a wide impedance bandwidth and stable radiation characteristics. Etching slots into both the radiating element and ground plane enables the precise control of current distribution, thereby enhancing operational bandwidth. The antenna was modeled and optimized in CST Microwave Studio and HFSS to ensure consistent simulation results. Experimental results demonstrate effective operation from 15 to 18 GHz, with a return loss (S_{11}) below -10 dB. The strong agreement between simulation and measurement results confirms the reliability of the design. The antenna's compact form factor and wideband performance make it suitable for satellite-on-the-move (SOTM) and low-Earth-orbit (LEO) terminal applications.

1. INTRODUCTION

As wireless communication systems continue to grow, there is a greater need for higher operational frequencies, particularly in the microwave and millimeter-wave bands. This trend is mainly driven by the rapid growth of next-generation satellite communication (SatCom) systems [1–3]. Modern services, such as high-speed satellite Internet, high-resolution Earth observation, and dense backhaul networks, require large bandwidth and high-capacity links. The Ku-band has become a key frequency range, balancing available bandwidth, manageable atmospheric attenuation, and system integration complexity [4, 5].

Microstrip patch antennas (MPAs) are extensively utilized in high-frequency planar technologies because of their low profile, ease of integration with monolithic microwave integrated circuit (MMIC) components, and cost-effectiveness [6, 7]. However, conventional MPAs exhibit inherent physical limitations, such as a narrow impedance bandwidth and relatively large size at lower microwave frequencies. As communication platforms shrink and accommodate multiple standards, these limitations pose significant challenges. Therefore, advanced electromagnetic techniques are required to enhance performance while maintaining antenna compactness [8, 9].

Defected structures provide a flexible and reliable approach to antenna engineering. A Defected Ground Structure (DGS) is formed by etching specific patterns into the ground plane, which alters the return current distribution [10, 11]. This modification alters the antenna's inductance-capacitance (LC) circuit parameters, resulting in an increased bandwidth, reduced size, and reduced surface-wave suppression [12, 13]. Additionally, DGS facilitates harmonic rejection and enhances isolation, both of which are critical for preserving signal integrity in densely populated satellite environments [14, 15].

In parallel with advancements in ground-plane engineering, Defected Microstrip Structures (DMSs) have gained prominence. Incorporating specific slots into the radiating element or feed line allows the DMS to provide precise control over guided-wave propagation [16, 17]. Unlike other filtering techniques, DMS enables resonance tuning and multiband operation without the need for external bulky components [18]. When properly optimized, DMS improves impedance matching and minimizes spurious radiation, making it suitable for high-density microwave circuits [19, 20].

Although DGS and DMS techniques are well established in antenna design, this study distinguishes itself by combining and optimizing their geometries. Consequently, the proposed single-element antenna demonstrates high efficiency, substantial gain, and compact dimensions, rendering it suitable for Ku-band satellite terminal applications.

This study presents a design that integrates DGS and DMS techniques to achieve high performance in Ku-band applications. The combination of these methods enables multiresonant behavior across the 15–18 GHz range while maintaining antenna compactness [21, 22]. The antenna was modeled using two numerical methods: the Finite Integration Technique (FIT) in Computer Simulation Technology (CST) Microwave Studio and the Finite Element Method (FEM) in Ansys High Frequency Structure Simulator (HFSS). This dual-modeling ap-

* Corresponding author: Rajae Tribak (tribak.rajae@etu.uae.ac.ma).

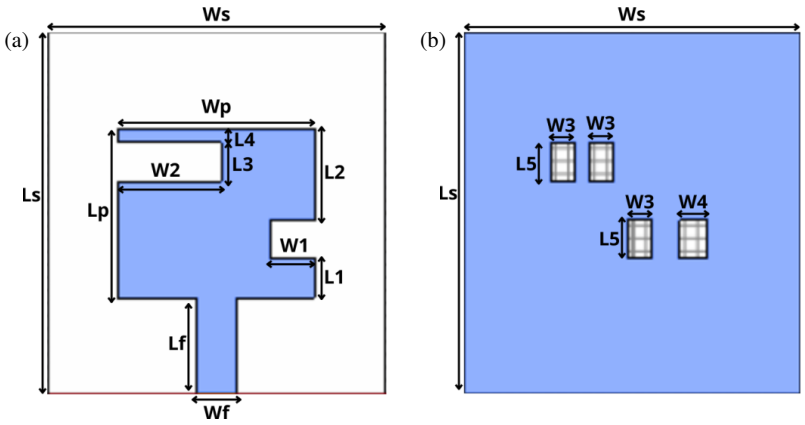

FIGURE 1. Geometry of the proposed wideband antenna: (a) Front view of the radiating patch with DMS slots. (b) Rear view of the ground plane with DGS patterns.

proach, supported by the experimental validation of the S_{11} parameters, substantiates the reliability of the results [23, 24]. The following sections describe the design methodology, present a parametric analysis of the defective structures, and provide final validation demonstrating the suitability of this design for modern satellite terminals.

2. ANTENNA DESIGN AND METHODOLOGY

A systematic methodology integrating analytical techniques with geometric optimization was used to develop the proposed Ku-band satellite and high-frequency wireless antenna. The design features a modified microstrip patch, incorporating defected microstrip structures on the radiating element and defected ground structures on the ground plane. Fig. 1 illustrates the overall geometry, and Table 1 lists the optimized parameters.

TABLE 1. Optimized geometrical parameters of the proposed antenna.

Parameter	Description	Value (mm)
L_s	Substrate Length	28
W_s	Substrate Width	26
L_p	Patch Length	13.1
W_p	Patch Width	15.3
L_f	Feed Line Length	8
W_f	Feed Line Width	3
h	Substrate Thickness	1.52
h_p	Copper Thickness	0.035
L_1	DMS Vertical segment 1	3
L_2	DMS Vertical segment 2	7.1
L_3	DMS Vertical slot height	3
L_4	DMS Vertical segment 3	1.1
L_5	DGS Slot length	3
W_1	DMS Horizontal slot width (Right)	3.4
W_2	DMS Horizontal slot width (Left)	8
W_3	DGS Slot width (Type 1)	1.8
W_4	DGS Slot width (Type 2)	2

2.1. Substrate Selection and Feed Mechanism

The electrical and radiation performance of a microstrip patch antenna is strongly influenced by the dielectric properties of its substrate [25]. In high-frequency applications, there is a trade-off among the antenna size, bandwidth, and radiation efficiency. Substrates with low dielectric constants and increased thickness can enhance the bandwidth and efficiency, although they result in larger antenna dimensions. Conversely, substrates with higher permittivity enable antenna miniaturization but reduce the bandwidth.

In this research, the proposed radiator was designed and fabricated on a high-frequency Rogers RO4003C dielectric substrate. This material was selected for its superior electrical stability and low-loss characteristics, with $\varepsilon_r = 3.38$, $h = 1.52$ mm, and $\tan\delta \approx 0.0027$. Both the radiating patch and defective ground plane consist of copper layers with a standard thickness of $h_p = 0.035$ mm. The Rogers RO4003C offers an optimal compromise between compactness and the wide impedance bandwidth required for robust Ku-band operation. To ensure efficient power transfer and seamless integration with standard radio frequency (RF) measurement equipment, the antenna was excited using a 50 Ω microstrip feedline with a width $W_f = 3$ mm and length $L_f = 8$ mm. Furthermore, impedance matching is meticulously refined by optimizing the inset feed position, effectively compensating for the parasitic reactances and fringing fields at the patch-to-line transition.

2.2. Geometric Design Formulation

The initial dimensions of the rectangular patch were determined using a well-known transmission line model. This model provides a reliable first estimate for microstrip antennas [6, 7]. The width of the patch (W_p) is a critical parameter that influences the antenna radiation and input impedance, and is calculated as follows:

$$W = \frac{v_0}{2f_r}\sqrt{\frac{2}{\epsilon_r + 1}} \tag{1}$$

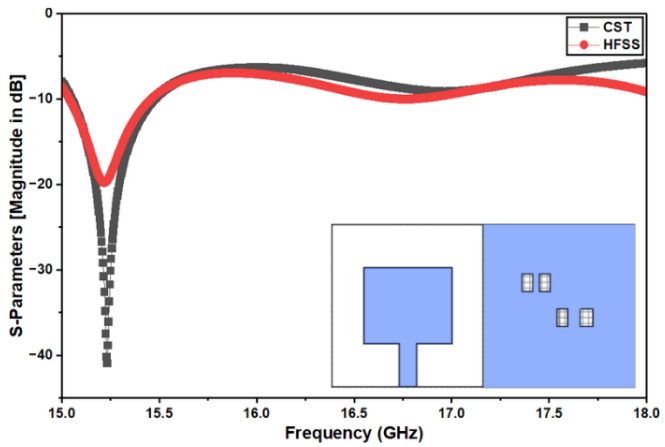

FIGURE 2. Effect of the DGS slot dimensions on the reflection coefficient of the proposed antenna.

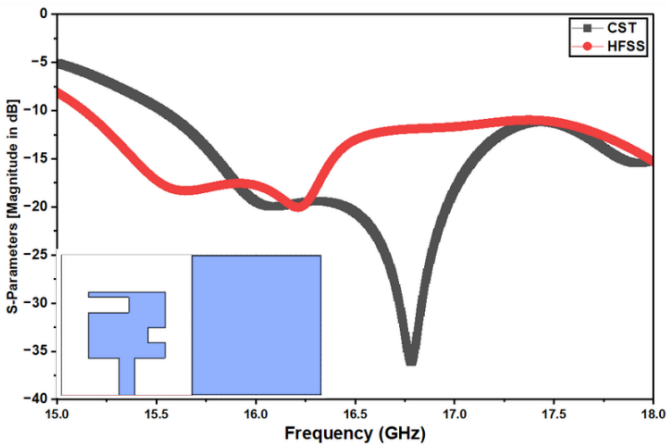

FIGURE 3. Influence of the DMS geometry on resonance tuning and multiresonant behavior of the antenna.

where v_0 denotes the velocity of light in free space (3×10^8 m/s); f_r is the desired resonant frequency; and ϵ_r represents the substrate dielectric constant.

Owing to the fringing fields at the patch edges, the antenna behaves electrically larger than its physical dimensions. This phenomenon is accounted for by introducing the effective dielectric constant ϵ_{reff} and the length extension ΔL, expressed as [7]:

$$\epsilon_{reff} = \frac{\epsilon_r + 1}{2} + \frac{\epsilon_r - 1}{2}\left[1 + 12\frac{h}{W}\right]^{-\frac{1}{2}} \tag{2}$$

$$\Delta L = 0.412h\frac{(\epsilon_{reff} + 0.3)\left(\frac{W}{h} + 0.264\right)}{(\epsilon_{reff} - 0.258)\left(\frac{W}{h} + 0.8\right)} \tag{3}$$

where h denotes the substrate thickness. Consequently, the effective length (L_{eff}) and actual physical length (L) of the patch are obtained as [6]:

$$L_{eff} = \frac{c}{2f_r\sqrt{\epsilon_{reff}}} \tag{4}$$

$$L = L_{eff} - 2\Delta L \tag{5}$$

These expressions establish the baseline geometry (13.1×15.3 mm), which is subsequently refined through numerical optimization to satisfy the stringent impedance bandwidth and matching requirements of Ku-band satellite terminals [3, 5].

2.3. Integration of DGS and DMS Techniques

To overcome the limited bandwidth of conventional microstrip patch antennas, the proposed design incorporates defected ground and defected microstrip structure techniques, as illustrated in Fig. 1 [10].

The DMS technique is implemented by etching complex slots into the radiating patch (W_1, W_2, and L_1–L_4). These slots alter the surface current distribution and introduce additional resonant paths, thereby enhancing the impedance bandwidth of the antenna. This approach results in the observed multiresonant behavior within the 15–18 GHz frequency range.

Simultaneously, the DGS is formed by etching rectangular slot patterns (W_3, W_4, L_5) in the ground plane, as depicted in Fig. 1(b). This configuration alters the return current path and modifies the equivalent inductance-capacitance (LC) characteristics. The combined use of DGS and DMS significantly enhanced the bandwidth, stability, and radiation efficiency of the antenna within the target frequency bands.

3. PARAMETRIC INVESTIGATION

The effects of structural modifications on antenna performance were evaluated to achieve optimal impedance matching in the Ku-band. This section examines the influence of defective structures on the resonance characteristics through a systematic parametric study.

3.1. Influence of DGS Slot Dimensions

This section examines the influence of the slot dimensions in the Defected Ground Structure on the impedance bandwidth. As illustrated in Fig. 2, variations in the widths W_3 and W_4, as well as the length L_5 of the etched slots in the ground plane, substantially affect the reflection coefficient (S_{11}) characteristics.

The incorporation of these DGS elements alters the surface current distribution and effectively inductive-capacitive (LC) loading of the antenna structure [10, 13]. This modification enables the controlled adjustment of the resonance depth and operational bandwidth [11, 18]. A parametric study demonstrated that the precise selection of DGS slot dimensions can enhance the bandwidth without increasing the antenna size [12, 22]. These findings underscore the importance of ground-plane design in achieving the wideband performance required for satellite communication terminals [14].

3.2. Effect of DMS Geometry on Resonance Tuning

This section analyzes the influence of the Defected Microstrip Structure geometry on resonance tuning and multiresonant behavior. As illustrated in Fig. 3, modifying the slot dimensions

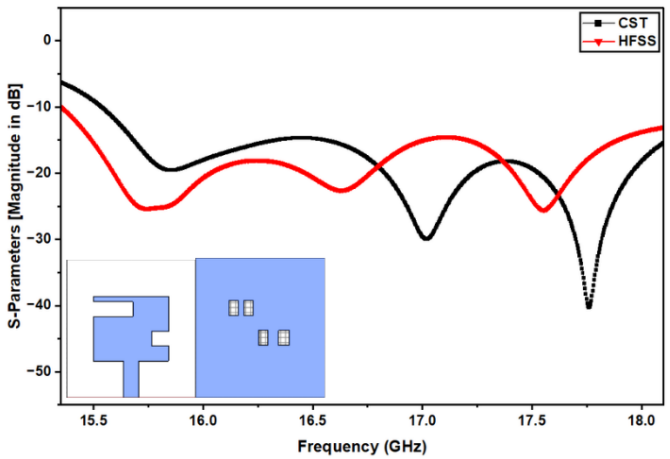

FIGURE 4. Simulated reflection coefficient illustrating the combined impact of DGS and DMS integration.

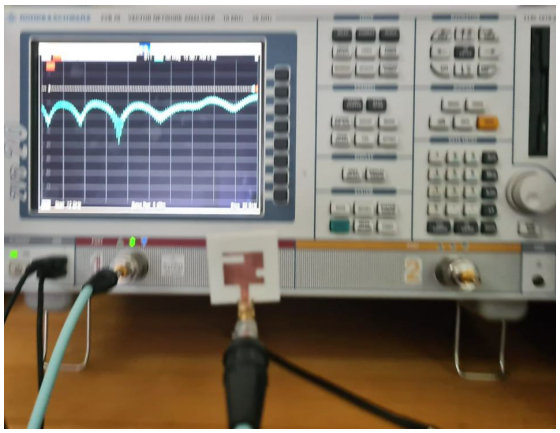

FIGURE 5. Measurement setup of the proposed antenna using a vector network analyzer (VNA).

of the radiating patch, particularly the horizontal widths W_1 and W_2 and the vertical segments L_1–L_4, directly alters the electrical current path length.

Introducing these specific defects into the patch surface causes the surface current to follow a longer and more complex path. This modification increases the electrical length of the radiator without increasing its physical dimensions [6, 12, 26]. Consequently, the primary resonant frequencies shift, and additional resonant modes emerge within the 15–18 GHz range, as demonstrated by the S_{11} comparison [18, 19, 27]. The DMS configuration provides a flexible approach for controlling the multiband characteristics of antennas, enabling the adjustment of the operating bands while maintaining stable performance for Ku-band satellite applications [5, 28, 29].

3.3. Synergistic Effect of Combined DGS and DMS Configurations

In the final phase of the parametric study, the defected microstrip structure and defected ground structure were integrated simultaneously to achieve an ultra-wideband (UWB) response. Individually, each structure primarily contributes to resonance tuning and impedance matching; however, their combined implementation stabilizes the reflection coefficient across the entire frequency range. As illustrated in Fig. 4, this hybrid configuration merges multiple resonant modes, particularly within the 15–18 GHz range, ensuring that S_{11} remains below -10 dB throughout.

The simulation results obtained from CST Microwave Studio and Ansys HFSS were in close agreement, thereby validating the robustness of the optimized design. The implementation of a dual-defect approach in conjunction with a low-loss Rogers RO4003C substrate enables the antenna to effectively mitigate reactive effects and maintain high radiation efficiency. The consistency between the two simulation tools indicates that the proposed geometry is suitable for subsequent experimental validation.

4. EXPERIMENTAL RESULTS AND COMPARATIVE ANALYSIS

To evaluate the effectiveness of the proposed design, a prototype was constructed and tested in a laboratory. This section describes the experimental setup and compares the numerical results with the corresponding measurements.

4.1. Experimental Setup and Measurement Procedure

The experimental validation commenced with the fabrication of the optimized antenna design on a Rogers RO4003C substrate. Fig. 6 shows the prototype, which incorporates DMS slots on the top patch and DGS elements on the ground plane. The compactness of the design was demonstrated by comparing it with a standard coin. For testing purposes, a 50 Ω SMA connector was soldered to the microstrip feedline.

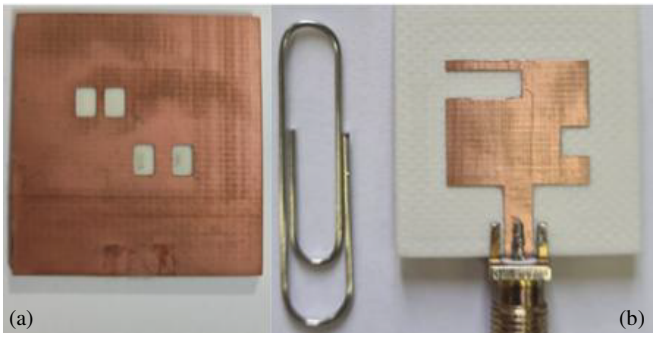

FIGURE 6. Fabricated prototype of the antenna: (a) radiating patch with DMS, (b) ground plane with DGS.

The reflection coefficient (S_{11}) was measured using a Vector Network Analyzer (VNA). Prior to the measurement, a standard Short, Open, Load, Through (SOLT) calibration was performed to eliminate parasitic effects from cables and connectors. The antenna was connected to the VNA port, as illustrated in the measurement setup in Fig. 5, and data were recorded across the 15–18 GHz frequency range. All measurements were per-

TABLE 2. Numerical and experimental performance comparison.

Method	f_{r1} (GHz)/S_{11} (dB)	f_{r2} (GHz)/S_{11} (dB)	f_{r3} (GHz)/S_{11} (dB)
CST Studio	15.6/−23.3	17.0/−30	17.8/−40.3
Ansys HFSS	15.7/−25.3	16.6/−22.6	17.55/−25.6
Measurement	15.5/−22.9	16.5/−22.1	17.82/−27.5

formed in a controlled laboratory environment to ensure accuracy and repeatability.

4.2. Comparative Analysis of Simulated and Measured S_{11}

The performance of the proposed antenna was validated by comparing the experimental data with the numerical results obtained from CST Microwave Studio and Ansys HFSS. As illustrated in Fig. 7, the measured reflection coefficient closely matches the simulated models, maintaining an impedance bandwidth ($S_{11} < -10$ dB) from 15.3 to 18.1 GHz. These findings indicate that integrating the DMS on the patch and the DGS on the ground plane achieves the desired wideband behavior.

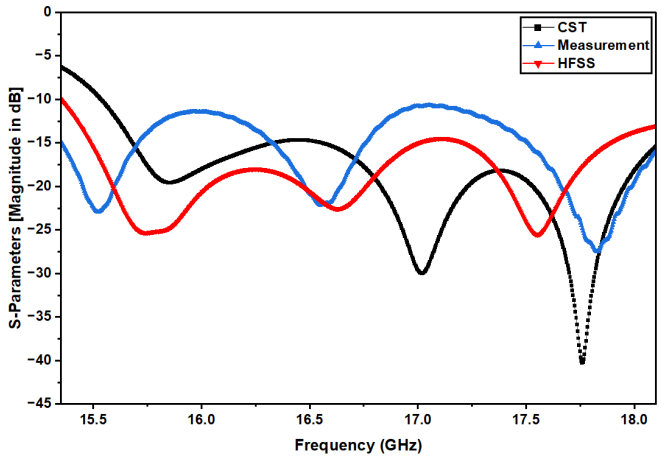

FIGURE 7. Comparison of simulated and measured reflection coefficients for the optimized antenna.

Although the results generally corresponded well, some discrepancies existed between the simulations and measurements. Such differences are typical in high-frequency designs and can be attributed to several factors.

- Fabrication Tolerances: Minor variations in the chemical etching of the DMS and DGS slots may alter the current path, resulting in slight shifts in the resonant frequencies.
- SMA Connector and Soldering: While simulations model ports as ideal transitions, practical implementation introduces parasitic reactances and minor losses owing to the soldering of the SMA connector.
- Substrate Variations: The actual dielectric constant and loss tangent of the Rogers RO4003C substrate may deviate slightly from the values assumed in the simulation software, particularly at higher Ku-band frequencies.
- Numerical Methods: Minor differences between the two software results arise from their distinct mathematical approaches. CST employs a Time Domain solver, whereas HFSS utilizes a Frequency Domain (Finite Element Method) solver. Each software package addresses mesh generation and boundary conditions differently.

Despite these variations, the measured results confirmed that the antenna was robust and met the specifications required for satellite applications.

The measurement equipment, including the VNA and anechoic chamber setup, has an accuracy tolerance of approximately 5%. To account for this limitation and prevent the appearance of unwarranted precision, all numerical and experimental results presented in the tables and text have been rounded accordingly.

Table 2 presents the specific resonant frequencies (f_r) and their corresponding return-loss magnitudes for detailed evaluation.

4.3. Radiation Performance, Gain, and Efficiency Analysis

The far-field characteristics of the proposed antenna were systematically evaluated to demonstrate its practical utility. This section examines the radiation patterns, gain, and radiation efficiency to verify that the combined DMS and DGS structures maintain high performance across the Ku-band.

Figure 8 shows the E- and H-plane radiation patterns of the antenna at several key frequencies within the Ku-band. The patterns at 15.6 GHz (CST), 15.7 GHz (HFSS), 16.6 GHz (HFSS), 17.0 GHz (CST), 17.6 GHz (HFSS), and 17.8 GHz (CST) were analyzed to provide a comprehensive overview of the antenna's performance across its operational range.

The results indicate that the antenna maintained stable radiation characteristics throughout the band. The H-plane exhibited a predominantly directional pattern, whereas the E-plane demonstrated greater focus and directivity. Small distortions or asymmetries became more pronounced at higher frequencies, particularly near 17.8 GHz. These effects are typical of this design and are generally attributed to the higher-order modes and the influence of the integrated DGS and DMS slots.

Although minor variations were observed at the higher end of the spectrum, the main beam remained stable. This stability demonstrates that the design preserves the radiation integrity within a compact structure. Therefore, the proposed antenna is a practical and reliable solution for Ku-band satellite terminals and high-frequency wireless applications.

The simulated gain of the proposed antenna remained steady across the Ku-band, primarily ranging from 5.5 to 9.2 dB. Fig. 9

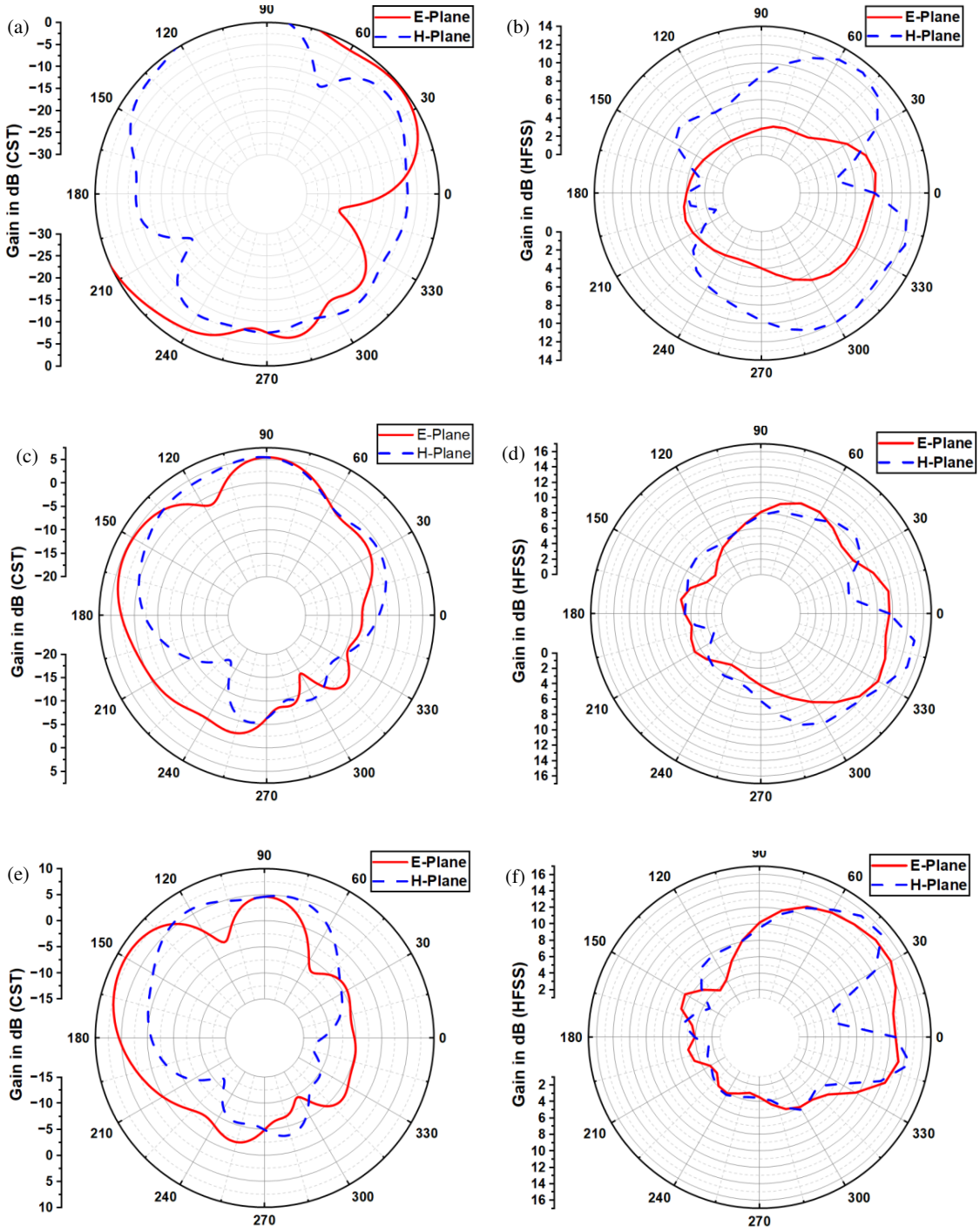

FIGURE 8. Comparison of simulated E-plane and H-plane radiation patterns at the three primary resonances: (a) 15.6 GHz, (b) 15.7 GHz, (c) 17.0 GHz, (d) 16.6 GHz, (e) 17.8 GHz and (f) 17.6 GHz.

demonstrates a clear increase in gain at higher frequencies, with a maximum of approximately 9.2 dB at 17.8 GHz in the CST simulation. The HFSS solver yielded a slightly lower peak of 6.5 dB at 17.6 GHz. Minor discrepancies between the two simulation tools, particularly above 17 GHz, are anticipated owing to differences in the numerical methods and meshing techniques. Despite these variations, the results indicate that the antenna design is robust and capable of reliable performance in high-frequency communications.

The efficiency results indicate that the proposed structure is effective. As shown in Fig. 10 and the comparative table, the radiation efficiency remained high across the entire frequency band, consistently exceeding 97% and reaching 98% in the HFSS simulations. These findings demonstrate that the dielectric and conductor losses are effectively managed, even with the inclusion of DGS and DMS features.

The total efficiency increases with frequency, as indicated by the CST results, rising from 61% at 15.6 GHz to a maximum

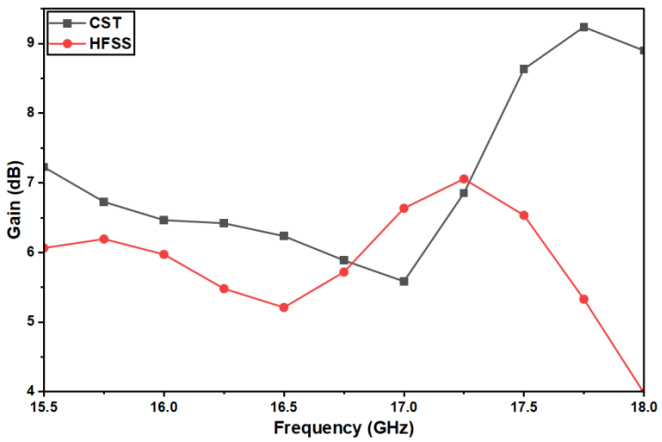

FIGURE 9. Gain variation of the antenna as a function of frequency obtained from CST and HFSS simulations.

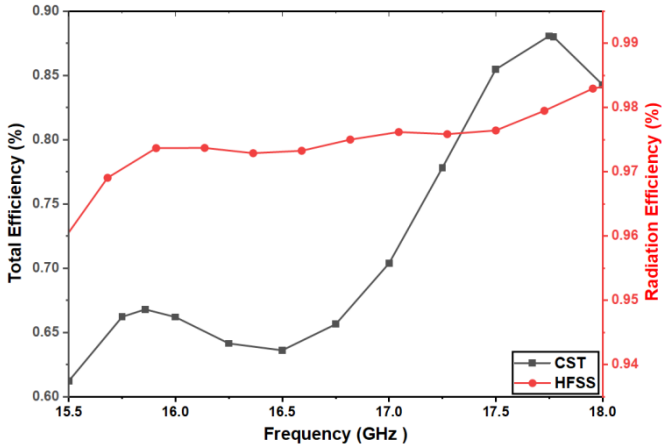

FIGURE 10. Simulated efficiency of the proposed antenna versus frequency with CST and HFSS.

TABLE 3. Comparison of simulated gain and efficiency at resonant frequencies.

Solver	CST	HFSS	CST	HFSS	CST	HFSS
Frequency (GHz)	15.6	15.7	17.0	16.6	17.8	17.6
Efficiency (%)	61	97	70	97	88	98
Gain (dB)	7.2	6.2	5.6	5.7	9.2	6.5

TABLE 4. Comparison of the proposed antenna with existing literature.

Reference	**Operating Bands (GHz)**	**Size (mm × mm)**	**Peak Gain (dBi)**	**Peak Efficiency (%)**	**Application**
[5]	16/30	8 × 8	8.0	-	Ku/Ka-band
[12]	3.6/5.6/7.4	30 × 24.8	2.0	92	WiMAX/X-band
[28]	2.4/7.9/10.7/17.6	31 × 27	7.3	79	S, C, X, and Ku-band
[29]	14.9	40 × 40	6.1	62	Ku-band
This Work	**15.5/16.5/17.8**	**26 × 28**	**9.2**	**96**	**Ku-band**

of 88% at 17.8 GHz. These findings suggest that the defective structures enhance impedance matching at higher frequencies while preserving a favorable radiation performance. Collectively, the results indicate that the antenna is suitable for Ku-band satellite applications, where high efficiency and effective power utilization are critical requirements.

Table 3 presents the primary performance metrics of the antenna at its resonant frequencies, providing a concise summary of its performance capabilities. The results indicate that the CST and Ansys HFSS solvers yield comparable gain and efficiency values.

Table 3 demonstrates the robust performance across the Ku-band. Notably, a peak gain of 9.2 dB was observed at the third resonance (17.8 GHz), which corresponds to a substantial increase in the total efficiency in the CST model.

The HFSS results indicated high radiation efficiency, with values exceeding 96% at all resonance points. While the two solvers exhibit minor discrepancies in resonance frequencies, particularly at the second resonance, the overall behavior of the antenna remains consistent.

The data indicate that the implementation of Defected Ground Structures and Defected Microstrip Structures was effective [8, 22]. These features enhanced impedance matching in the targeted areas, resulting in a favorable balance of high gain and efficiency within a compact design [27, 30]. These findings provide a justification for advancing to the hardware prototype stage for Ku-band satellite applications.

A comparative analysis with recently published single-element antennas operating in similar frequency bands is presented in Table 4 to emphasize the advantages of the proposed design. The comparison considers physical dimensions, peak gain, and radiation efficiency. As shown in Table 4, the proposed combined DGS and DMS configuration achieves the highest peak gain (9.2 dBi) and peak efficiency (96%) among the referenced works. Additionally, it maintains a compact

footprint of $26 \times 28\,\text{mm}^2$, which makes it highly competitive and suitable for Ku-band satellite communication systems.

The proposed single-element antenna demonstrates satisfactory performance; however, it does not achieve the directivity and gain observed in multi-element designs. Future research should investigate the adaptation of this optimized DGS-DMS design for integration into a multiple-input multiple-output (MIMO) antenna system. Such an approach is expected to enhance gain, spatial isolation, and channel capacity, thereby increasing the antenna's effectiveness for advanced satellite communication applications.

5. CONCLUSION

This study presents the design and testing of a high-performance, compact Ku-band antenna. The implementation of defected ground and microstrip structures enabled a reduction in the antenna size while maintaining the radiation performance.

The numerical analyses conducted using both CST and HFSS solvers demonstrated consistent results. The antenna achieved a peak gain of 9.2 dB and maintained a radiation efficiency above 96%.

The experimental results substantiate the practical value of this design. The measured S_{11} parameters exhibited a strong agreement with the simulated predictions, confirming effective impedance matching under real-world conditions. This alignment between the theoretical and experimental outcomes indicates that the proposed antenna offers a reliable and efficient solution for modern satellite terminals and high-frequency communication systems, particularly in contexts where power efficiency and size reduction are essential.

REFERENCES

[1] Palepu, N. R., J. Kumar, S. Peddakrishna, and A. Ghosh, "Wideband meander-line-antipodal-Vivaldi slot-antenna for millimeter-wave applications," *e-Prime — Advances in Electrical Engineering, Electronics and Energy*, Vol. 9, 100641, Sep. 2024.

[2] Pourmohammadi, P., H. Naseri, N. Melouki, F. Ahmed, Q. Zheng, A. Iqbal, and T. A. Denidni, "A wideband beam steering transmitarray antenna for Ka-band applications," *AEU — International Journal of Electronics and Communications*, Vol. 193, 155720, Mar. 2025.

[3] Truong, N., S. Das, S. K. Sharma, J.-C. S. Chieh, R. Farkouh, and G. M. Rebeiz, "Wideband circularly polarized array antenna using a novel radiating element for X-/Ku-band SATCOM," *IEEE Antennas and Wireless Propagation Letters*, Vol. 25, No. 1, 299–303, Jan. 2026.

[4] Pavone, S. C., G. S. Mauro, L. D. Donato, and G. Sorbello, "Design of dual circularly polarized sequentially-fed patch antennas for satellite applications," *Applied Sciences*, Vol. 10, No. 6, 2107, Mar. 2020.

[5] Kandwal, A., "Compact dual band antenna design for Ku/Ka band applications," *Advanced Electromagnetics*, Vol. 6, No. 4, 1–5, 2017.

[6] Wong, K.-L., *Compact and Broadband Microstrip Antennas*, John Wiley & Sons, 2002.

[7] Garg, R., P. Bhartia, I. Bahi, and A. Ittpiboon, *Microstrip Antenna Design Handbook*, Artech House, 2001.

[8] Sabbar, N., M. A. Ennasar, and L. Setti, "A new multi wideband monopole antenna using miniaturized technique for 5G, medical and radars (satellite) applications," in *7th International Conference on Advanced Technologies for Humanity*, 177–189, Kenitra, Morocco, 2025.

[9] Nhlengethwa, N. L. and P. Kumar, "Fractal microstrip patch antennas for dual-band and triple-band wireless applications," *International Journal on Smart Sensing and Intelligent Systems*, Vol. 14, No. 1, 1–9, 2021.

[10] Yang, F. and Y. Rahmat-Samii, *Electromagnetic Band Gap Structures in Antenna Engineering*, Cambridge University Press, 2009.

[11] Deng, Z.-B., W. Jiang, S.-X. Gong, Y.-X. Xu, and Y. Zhang, "A new method for broadening bandwidths of circular polarized microstrip antennas by using DGS & parasitic split-ring resonators," *Progress In Electromagnetics Research*, Vol. 136, 739–751, 2013.

[12] Ali, T., M. S. AW, R. C. Biradar, A. Andújar, and J. Anguera, "A miniaturized slotted ground structure UWB antenna for multiband applications," *Microwave and Optical Technology Letters*, Vol. 60, No. 8, 2060–2068, Aug. 2018.

[13] Veisee, S., S. Asadi, and M. K. Hedayati, "A novel compact defected ground structure and its application in mutual coupling reduction of a microstrip antenna," *Turkish Journal of Electrical Engineering and Computer Sciences*, Vol. 24, No. 5, 3664–3670, 2016.

[14] El Ouahabi, M., A. Dkiouak, A. Zakriti, M. Essaaidi, and H. Elftouh, "Analysis and design of a compact ultra-wideband antenna with WLAN and X-band satellite notch," *International Journal of Electrical and Computer Engineering (IJECE)*, Vol. 10, No. 4, 4261–4269, 2020.

[15] Elkorany, A. S., G. T. Ahmed, and D. A. Saleeb, "A planar UWB antenna with dual band rejection capability using double rotated ESRRs," *Advanced Electromagnetics*, Vol. 7, No. 1, 19–24, 2018.

[16] Jha, P., S. Singh, and R. L. Yadava, "Wideband sub-6 GHz microstrip antenna: Design and fabrication," *Advances in Smart Communication and Imaging Systems: Select Proceedings of MedCom 2020*, Vol. 721, 109–115, 2021.

[17] Ashish, J. and A. P. Rao, "Design and implementation of compact dual band U-slot microstrip antenna for 2.4 GHz WLAN and 3.5 GHz WiMAX applications," in *2019 International Conference on Smart Systems and Inventive Technology (ICSSIT)*, 1084–1086, Tirunelveli, India, Nov. 2019.

[18] Boutejdar, A., M. Challal, S. D. Bennani, F. Mouhouche, and K. Djafri, "Design and fabrication of a novel quadruple-band monopole antenna using a U-DGS and open-loop-ring resonators," *Advanced Electromagnetics*, Vol. 6, No. 3, 59–63, 2017.

[19] Shandal, S., Y. S. Mezaal, M. Kadim, and M. Mosleh, "New compact wideband microstrip antenna for wireless applications," *Advanced Electromagnetics*, Vol. 7, No. 4, 85–92, 2018.

[20] Bembarka, A., L. Setti, A. Tribak, H. Tizyi, and M. El Ouahabi, "A novel wideband beamforming antenna for 5G applications by eliminating the phase shifters and crossovers from the Butler matrix," *Progress In Electromagnetics Research C*, Vol. 133, 51–63, 2023.

[21] Saeed, M. A. and A. O. Nwajana, "Design of a rectangular linear microstrip patch antenna array for 5G communication," in *2024 IEEE International Symposium on Phased Array Systems and Technology (ARRAY)*, 1–4, Boston, MA, USA, 2024.

[22] Singh, R. K., A. Kumar, and A. Aboulqasim, "Comparative analysis of triangular grid with ground defected microstrip patch antennas," *International Journal of Intelligent Systems and Applications in Engineering*, Vol. 12, No. 22s, 1723, 2024.

[23] Kaur, S., R. Khanna, P. Sahni, and N. Kumar, "Design and optimization of microstrip patch antenna using artificial neural networks," *International Journal of Innovative Technology and Exploring Engineering*, Vol. 8, No. 9, 611–616, Jul. 2019.

[24] Olawoye, T. O. and P. Kumar, "A high gain microstrip patch antenna with slotted ground plane for sub-6 GHz 5G communications," in *2020 International Conference on Artificial Intelligence, Big Data, Computing and Data Communication Systems (icABCD)*, 1–6, Durban, South Africa, 2020.

[25] Alumari, I., M. D. H. Almawlawe, Z. H. Al-Araji, and V. G. Saitkulov, "Impact of substrate dielectric constant on performance of 2.4 GHz microstrip patch antenna array," *Wasit Journal of Engineering Sciences*, Vol. 13, No. 1, 22–38, Mar. 2025.

[26] Er-Rebyiy, R., J. Zbitou, M. Latrach, A. Tajmouati, A. Errkik, and L. El Abdellaoui, "New miniature planar microstrip antenna using DGS for ISM applications," *Telkomnika (Telecommunication Computing Electronics and Control)*, Vol. 15, No. 3, 1149–1154, 2017.

[27] Sharma, A., A. Bhardwaj, M. I. Khan, M. G. Siddiqui, S. Bhaskar, and Kamakshi, "High-performance octagonal multiband microstrip antenna with DGS for 5G networks and iot integration," *African Journal of Biomedical Research*, Vol. 27, No. 6S, 1716–1723, Dec. 2024.

[28] Shuriji, M. A. and R. H. Thaher, "Design of new tuning circuit based reconfigurable microstrip antenna for S, C, X, and Ku bands applications," *Journal of the Chinese Institute of Engineers*, Vol. 47, No. 4, 399–404, 2024.

[29] Ravi, L., R. Srilakshmi, and P. V. Nagalakshmi, "Advancements in microstrip patch antenna design for satellite applications," *International Journal of Creative Research Thoughts (IJCRT)*, Vol. 12, No. 4, 239–244, 2024.

[30] Ahmed, M. F. and M. H. Kabir, "An analysis of methods for enhancing gain and bandwidth in ultra-wideband microstrip patch antennas," *Cureus Journal of Engineering*, 1–14, May 2025.